

# Investigation of temperature sensitivity of a MEMS gravimeter based on geometric anti-spring

Cite as: Rev. Sci. Instrum. **93**, 125002 (2022); <https://doi.org/10.1063/5.0114664>

Submitted: 26 July 2022 • Accepted: 11 November 2022 • Published Online: 01 December 2022

Published open access through an agreement with University of Glasgow Faculty of Information and Mathematical Sciences

 Vinod Belwanshi, Abhinav Prasad, Karl Toland, et al.



View Online



Export Citation



CrossMark

## ARTICLES YOU MAY BE INTERESTED IN

[Physical simulation technologies and testing system for cavern shape control from single-well solution mining in rock salt](#)

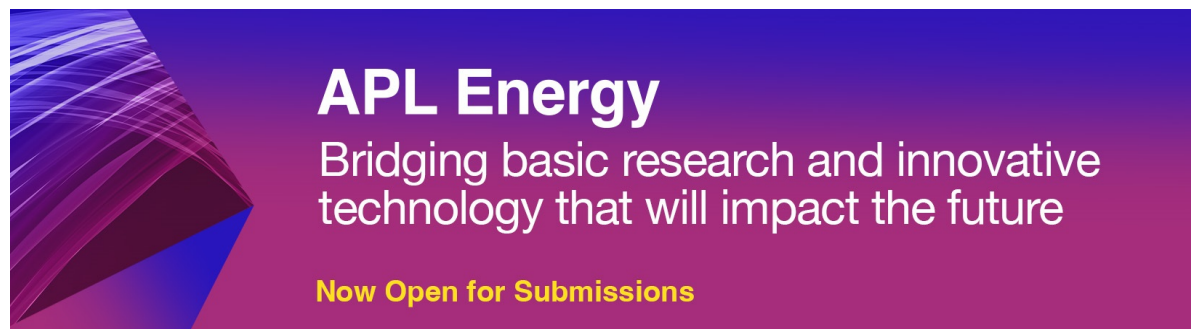
Review of Scientific Instruments **93**, 125101 (2022); <https://doi.org/10.1063/5.0108039>

[Performance improvement of space-resolved extreme ultraviolet spectrometer by use of complementary metal-oxide semiconductor detectors at the Experimental Advanced Superconducting Tokamak](#)

Review of Scientific Instruments **93**, 123501 (2022); <https://doi.org/10.1063/5.0104225>

[Dual-mode acceleration sensor of downhole drilling tools based on triboelectric nanogenerator](#)

Review of Scientific Instruments **93**, 125001 (2022); <https://doi.org/10.1063/5.0121965>



**APL Energy**  
Bridging basic research and innovative  
technology that will impact the future  
**Now Open for Submissions**

# Investigation of temperature sensitivity of a MEMS gravimeter based on geometric anti-spring

Cite as: Rev. Sci. Instrum. 93, 125002 (2022); doi: 10.1063/5.0114664

Submitted: 26 July 2022 • Accepted: 11 November 2022 •

Published Online: 1 December 2022



View Online



Export Citation



CrossMark

Vinod Belwanshi,<sup>1,a)</sup>  Abhinav Prasad,<sup>1</sup> Karl Toland,<sup>1</sup> Richard Middlemiss,<sup>1</sup>  Douglas Paul,<sup>2</sup>   
and Giles Hammond<sup>1</sup>

## AFFILIATIONS

<sup>1</sup>Institute for Gravitational Research, School of Physics and Astronomy, University of Glasgow, Glasgow G12 8QQ, United Kingdom

<sup>2</sup>James Watt School of Engineering, School of Engineering, University of Glasgow, Glasgow G12 8LT, United Kingdom

<sup>a)</sup>Author to whom correspondence should be addressed: [vinod.belwanshi@glasgow.ac.uk](mailto:vinod.belwanshi@glasgow.ac.uk)

## ABSTRACT

This paper describes a technique for temperature sensitivity or thermal sag measurements of a geometric anti-spring based microelectromechanical system (MEMS) gravimeter (Wee-g). The Wee-g MEMS gravimeter is currently fabricated on a (100) silicon wafer using standard micro-nano fabrication techniques. The thermal behavior of silicon indicates that the Young's modulus of silicon decreases with increase in temperature ( $\sim 64$  ppm/K). This leads to a softening of the silicon material, resulting in the proof mass displacing (or sagging) under the influence of increasing temperature. It results in a change in the measured gravity, which is expressed as temperature sensitivity in terms of change in gravity per degree temperature. The temperature sensitivity for the silicon based MEMS gravimeter is found to be 60.14–64.87, 61.76, and 62.76  $\mu\text{Gal}/\text{mK}$  for experimental, finite element analysis (FEA) simulation, and analytical calculations, respectively. It suggests that the gravimeter's temperature sensitivity is dependent on the material properties used to fabricate the MEMS devices. In this paper, the experimental measurements of thermal sag are presented along with analytical calculations and simulations of the effect using FEA. The bespoke optical measurement system to quantify the thermal sag is also described. The results presented are an essential step toward the development of temperature insensitive MEMS gravimeters.

© 2022 Author(s). All article content, except where otherwise noted, is licensed under a Creative Commons Attribution (CC BY) license (<http://creativecommons.org/licenses/by/4.0/>). <https://doi.org/10.1063/5.0114664>

## I. INTRODUCTION

Microelectromechanical system (MEMS) based silicon sensors have gained popularity in a variety of application areas and gravimetry is among them. The MEMS gravimeter, developed at Glasgow, utilizes geometrical anti-spring (GAS) based flexures to improve the device's acceleration sensitivity with low natural frequencies.<sup>1,2</sup> Such low-frequency and soft spring devices are also becoming more useful for tilt sensing and seismometers.<sup>3</sup> Low-frequency devices, however, are sensitive to temperature changes; hence, the stability of the sensor is significantly impacted by ambient temperature fluctuations.<sup>4</sup> Finite element analysis (FEA) is limited to provide a deviated estimate that are not close to actual performance of such devices. Thus, accurate characterization of these devices is needed particularly when manual packaging steps are being adopted, such as glued pickup glass plate on the MEMS gravimeter device. Temperature influenced effect is in part due to the negative linear temperature coefficient of Young's modulus

(TCE) of  $\sim -63.83$  ppm/ $^{\circ}\text{C}^{5-7}$  for silicon. A change in temperature leads to either the stiffening (when the temperature decreases) or softening (when the temperature increases) of flexure springs, causing a corresponding displacement of the proof mass (PM). Assuming the designed frequency of the MEMS gravimeter is 7.5 Hz, the proof mass sags 5.5  $\mu\text{m}$  with a 20  $^{\circ}\text{C}$  temperature increase, leading to a  $\sim 61.76$   $\mu\text{Gal}/\text{mK}$  spurious change in the measured gravity signal. This thermal sag becomes significantly important if the gravimeter needs to measure a gravity change on the order of 10 s of  $\mu\text{Gal}$ , which is often the case for surveying applications in gravimetry. In order to compensate for the thermal sag, it is necessary to quantify the effect so that an effective compensation technique can be implemented. To remove the impact of temperature from the measurements, one can either monitor the temperature and regress it out during the post-processing step or implement passive or active compensation techniques. All of these approaches, however, have their advantages/disadvantages that need to be considered before their implementation. Considering that GAS based MEMS designs

are gaining popularity in recent years,<sup>8,9</sup> it is crucial to understand the impact of temperature on such devices. While there has been some previous work on formulating the temperature sensitivity of GAS flexures used for test-mass suspensions in gravitational wave detectors,<sup>10,11</sup> a complimentary study for the MEMS scale designs has not been adequately covered. Here, the thermal sag of the proof mass with an increase in temperature is quantified using experimental, analytical, and FEA simulation calculation. Various measurement techniques have been demonstrated to measure thermal sag in other devices. Kamp<sup>12</sup> has demonstrated the measurement of a vertical seismic accelerometer deflection using a laser vibrometer with a 45° tilted mirror (a costlier technique). They have not, however, performed temperature induced sag measurements. Imperial College London used a laser source to measure the thermal sag of a vertical seismic accelerometer.<sup>13</sup> However, such a system needs a polished surface with a stable laser, hence leading to a complex technique for thermal sag measurement.

In this paper, we demonstrate a new approach with a simpler optical measurement system to measure the thermal sag of a MEMS gravimeter and verify the technique using both theoretical estimates and finite element analysis (FEA) simulations. The optical technique demonstrated in this paper is simpler and an alternative low-cost solution for thermal sag measurement. Such thermal measurements preclude the requirement of integrating a complete device using electronics and/or using more expensive instrumentation to be able to extract the thermal sensitivity of the device. Additionally, the current optical setup has the potential to measure displacements under 1 g (where  $g = 9.8066 \text{ ms}^{-2}$ ) loading in low-frequency devices before packaging and wire bonding. This information can also be used as a feedback to optimize the fabrication of devices. The rest of this paper is divided into the following sections: Sec. II contains an explanation of the analytical theory, Sec. III is an introduction to the thermal sag measurement setup used to conduct the work, Sec. IV presents a description of the results and discussions, and Sec. V outlines the major conclusions and future directions.

## II. THEORY

A GAS MEMS gravimeter consists of geometrical anti-spring-based flexures, a proof mass, and a frame as shown in Fig. 1. A photograph of the MEMS device [Fig. 1(a)] and its fabrication details can be accessed from Ref. 1, the packaged MEMS gravimeter is shown in Fig. 1(b),<sup>14</sup> and a simplified schematic diagram of the GAS MEMS gravimeter is presented in Fig. 1(c). Figure 1(c) also helps to visualize thermal sag under the influence of temperature at an acceleration of 1 g. The change in deflection of the proof mass can be explained using the following relation:

$$\Delta y_{eq} = \frac{\Delta F}{k_{eff}} = \frac{g\Delta m}{k_{eff}} = \frac{g\Delta m}{m\omega_0^2}, \quad (1)$$

where  $\Delta y_{eq}$  is the thermal sag due to change in temperature,  $\Delta F$  is the change in applied effective load due to temperature,  $m$  is the mass of the proof mass,  $\Delta m/m$  is a relative change in the proof mass that is equivalent to the relative change in Young's modulus of the material due to change in temperature,  $k_{eff}$  is the effective stiffness, and  $\omega_0$  is the angular resonant frequency of the device. It can be stated that

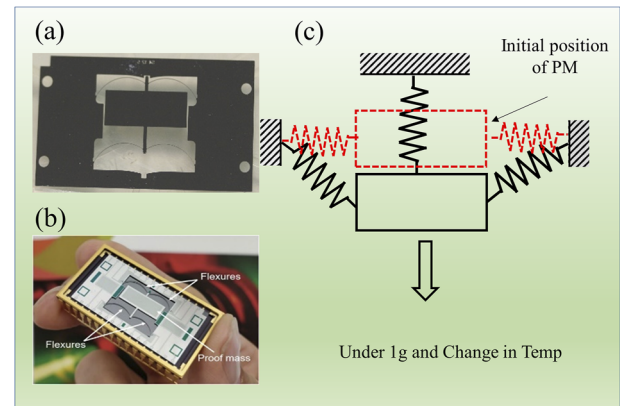


**FIG. 1.** (a) A photograph of the MEMS gravimeter used for thermal sag measurements, (b) a photograph of the packaged MEMS gravimeter [Reproduced with permission from Carbone *et al.*, *Front. Earth Sci.* 8, 573396 (2020). Copyright 2020, licensed under a Creative Commons Attribution (CC BY) license, and (c) a schematic diagram of the MEMS gravimeter under the influence of temperature.

$$\frac{\Delta y_{eq}}{\Delta T} = \left( \frac{g}{\omega_0^2} \right) \frac{\Delta E}{E\Delta T}. \quad (2)$$

A relative change,  $\Delta E/E$ , in the Young's modulus,  $E$ , due to a temperature change,  $\Delta T$ , is equivalent to a relative change in its load at fixed temperature:  $\Delta E/E = \Delta m/m$ .<sup>11</sup>

The tendency of silicon is to become soft under elevated temperatures and this leads to a change in the stiffness of silicon materials, which is responsible for the thermal sag of proof mass. Equation (2) was used for obtaining an analytical estimate of thermal sag vs frequency of the device and the estimate was found to be in close agreement with FEA and experimental data, which will be explained in the subsequent sections.

## III. THERMAL SAG EXPERIMENTAL SETUP

The MEMS gravimeter is operated vertically; hence, measuring the position of the proof mass becomes difficult using conventional instruments inside a clean room during fabrication. In addition, temperature induced effects in the MEMS gravimeter are required to be measured to understand the gravimeter's temperature sensitivity. The temperature needs to be increased in a controlled manner and the position of PM needs to be measured at different temperatures. To address this concern, an optical measurement system was developed as shown in Fig. 2, this was based upon the work of Toland.<sup>15</sup> The bespoke experimental setup consists of a Thorlabs high speed CMOS camera (Thorlabs DCC1240M) with 28× zoom optical lens (Thorlabs MVL12X20L, MVL20A, and MVL12X12Z) in order to image the position of the PM of the MEMS gravimeter, a heater (Thorlabs PTC-1) (which can be controlled remotely to increase and decrease the temperature), and a cold light source (KL 1500LCD) to illuminate the MEMS PM and frame. The setup was kept on top of a vibration isolation bench to avoid any external coupled vibration. Additionally, the MEMS, heater, and camera were covered using a transparent plastic box to avoid issues coupled with air current (Fig. 2).

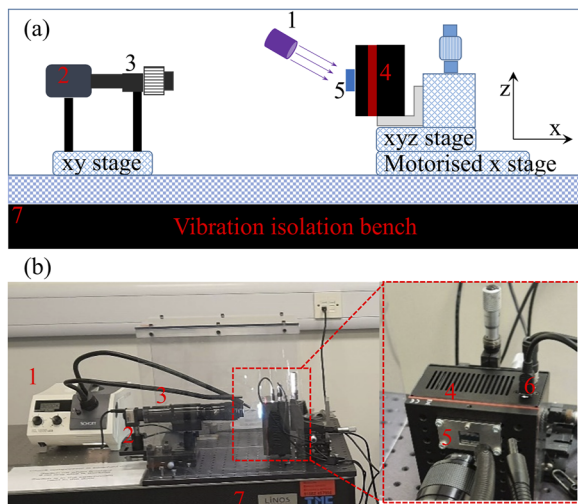


**FIG. 2.** (a) A schematic and (b) a photograph of the thermal sag measurement setup with an expanded view of the MEMS device on a heater: (1) a cold light source, (2) CMOS camera, (3) 28 $\times$  objective lens, (4) hot plate, (5) MEMS with a holding package, (6) to connect power supply and computer to hotplate, and (7) the vibration isolation bench. The temperature sensitivity of the setup is 0.3  $\mu\text{m}/\text{K}$  along the z-axis, which is nullified using differential measurements.

Remote access was used to record images using camera, to control the hot plate, and to move a motorized stage to adjust the focus. External disturbances from human interaction were therefore reduced.

In designing the setup, a few critical hurdles likely to reduce the efficacy of the apparatus were noted. The foremost was the thermal expansion coefficients of the materials used in the setup. During an initial test, a power resistor was utilized to increase the temperature of the MEMS, with the MEMS device placed on top of this power resistor using a slit made of two glass slides. The power resistor enclosure was made of aluminum; due to thermal expansion, the slit width was increased and, hence, the MEMS device started tilting. Due to the tilting, the effective gravity applied on the MEMS PM was slightly reduced and it was observed that the proof mass was increasing instead of decreasing with increase in temperature. It can be concluded that the tilting effect was more significant compared to the softening of the silicon material. To eliminate the tilting issue of the MEMS device, a package was fabricated using stainless steel to hold the MEMS and it was kept on top of the hotplate instead of the power resistor.

After this change, it was possible to see the thermal sag using the optical experimental setup based on differential measurements of the proof mass movement. The CMOS camera was first calibrated against a standard known diameter (25  $\mu\text{m}$ ) of wire and using a 28 $\times$  optical zoom objective lens, the system had a calibration factor of 0.19  $\mu\text{m}/\text{pixel}$ . The numerical aperture of the objective lens was 0.202 and working distance was 37 mm. The resolution of the CMOS camera was 1280  $\times$  1024 pixels. As per the calibration factor, the measurement setup can image an area of 243  $\times$  205  $\mu\text{m}^2$  of the MEMS device. During the course of measurements at two different temperatures, it was observed that it was possible to move the full MEMS device up or down due thermal expansion of the

package and hotplate. Hence, a differential measurement is required to quantify the thermal sag. It was possible to see the frame and proof mass of the MEMS device simultaneously, and the artifact spots on top of the MEMS device were utilized for differential measurements. The movement of the proof mass was recorded at 25 and 45  $^{\circ}\text{C}$  and the artifacts were tracked using the Fiji ImageJ software.<sup>16</sup> The results of the thermal sag experiments and temperature sensitivity are presented in Sec. IV.

#### IV. RESULTS AND DISCUSSIONS

The MEMS gravimeter was characterized using the experimental setup as explained in Sec. III. The thermal sag measurements were performed remotely overnight on the vibration isolation bench to avoid externally coupled vibrations. The movements of the proof mass at 25 and 45  $^{\circ}\text{C}$  were recorded and further analyzed to quantify the proof mass location using an open source ImageJ software for thermal sag of the MEMS gravimeter. Primarily, to understand measurement setup accuracy, the methodology used for thermal sag measurement has been repeated and presented. Multiple images (frames) of the MEMS with moving PM and supporting frame were

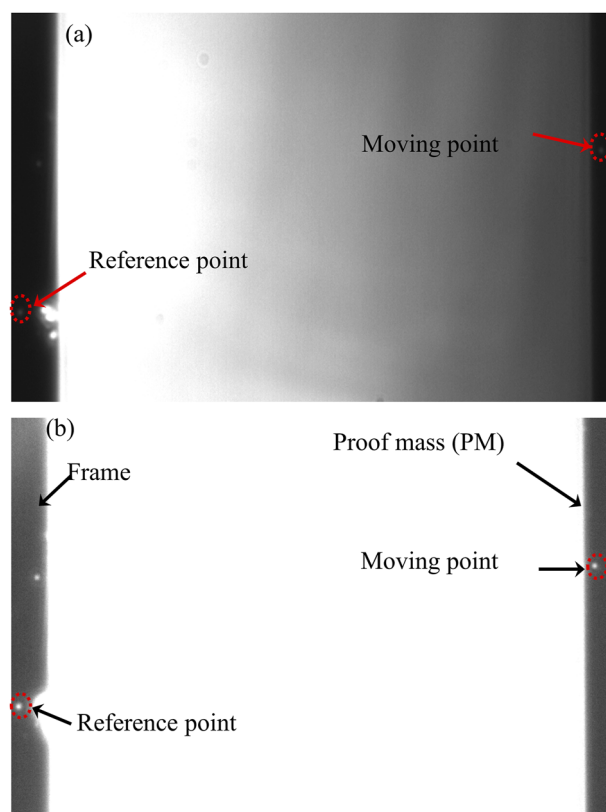


**FIG. 3.** (a) Actual and (b) linearly changed pixel intensity photographs for MEMS gravimeter having a moving PM (right) and a frame to attach the PM (left). Under 1 g loading, the proof mass continuously moves up and down because of ground vibration. The spot (red circle) on the left was used as a stationary reference and the spot (red circled) on the right was the moving point. The difference between these two points was then calculated.



recorded. The photographs with actual and linearly changed pixel intensity are presented in Figs. 3(a) and 3(b), respectively. Two points were selected on the MEMS: one on the frame as a reference and the second on the proof mass as a moving point. Both the points were tracked using the ImageJ software and the proof mass position was calculated with respect to the reference point by taking their difference.

The difference between the two points was calculated and plotted against the respective frames imaged for PM movement shown in Fig. 4(a), and a zoomed-in view for frame numbers 30–40 is presented in Fig. 4(b) to show variations in the amplitude of PM movement. This variation in amplitude is because of ground vibrations. Furthermore, the average position of PM with reference point was calculated and analyzed. It is observed that a deviation of  $\pm 0.85$  pixel ( $0.16 \mu\text{m}$ ) was calculated in the measured average position of PM with the reference position as shown in Fig. 4(c). Differential measurements were conducted to avoid movement of the full MEMS device due thermal expansion of the hot plate surface and/or the package used to hold the MEMS device. Figure 4(d) shows the PM positions in pixels for temperature at 25 and 45 °C, and the difference in the position of proof mass was calculated based on the  $0.19 \mu\text{m}/\text{pixel}$  calibration factor. Multiple MEMS gravimeter devices (named as MEMS 1, MEMS 2 MEMS 3, and MEMS 4) were characterized to locate the position of the proof mass with respect to the reference point at 25 and 45 °C.

The thermal sag of a MEMS device was analytically calculated as a function of resonant frequency and is presented in Fig. 5(a) by a black dashed curve. The MEMS devices investigated had frequencies ranging from 8 to 12 Hz. The frequency was reduced to 8.5 Hz by adding mass to the proof mass so that the behavior could be analyzed for a lower-frequency device. As can be seen in Fig. 5, the experimentally measured thermal sags were  $\sim 2\text{--}4 \mu\text{m}$  for devices under thermal sag investigation for a temperature change of 20 °C. A number of thermal sag experiments were conducted and the data analyzed are presented in Fig. 5 for all MEMS devices.

It can be seen that the experimental thermal sag measurements demonstrate good agreement with the analytical calculations and the ANSYS FEA simulation. For MEMS 1 (10 Hz device), the blue solid circle corresponds to thermal sag measurements carried out during the day-time without the vibration isolation bench. Day-time experiments produced higher amplitudes of movement of the proof mass due to externally coupled vibrations. Since differential measurements were carried out, these thermal sag experiments show good agreement with the estimated thermal sag. The issue of externally coupled vibrations was resolved by utilizing a vibration isolation bench with overnight measurements (red squares and purple triangles correspond to MEMS 2 and 3, respectively, of the 12 Hz device). The MEMS 4 8.5 Hz device was also characterized for thermal sag (star green point) [Fig. 5(a)]. Based on all experiments, it can be concluded that the device's thermal sag can be measured and the measurements demonstrate good agreement with the estimated thermal sag with a deviation of 1.68%, 3.26%, 11.96%, and 9.56% for MEMS 1, 2, 3, and 4, respectively. The temperature sensitivity was derived and is plotted in Fig. 5(b); it can be seen that the temperature sensitivity of silicon based MEMS gravimeter was 60.14–64.81, 61.76, and 62.76  $\mu\text{Gal}/\text{mK}$  for experimental, FEA simulation, and analytical calculations, respectively. It suggests that the temperature sensitivity of MEMS gravimeters is dependent on the

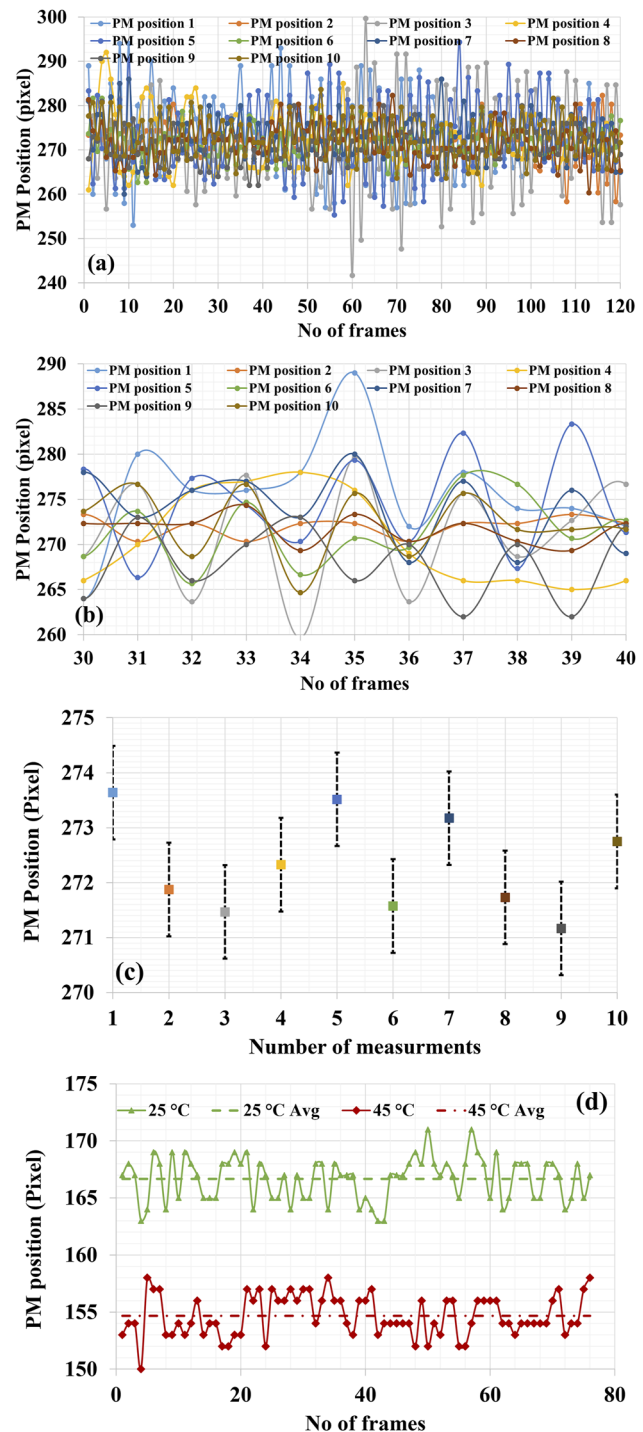


**FIG. 4.** (a) The ten measurements for PM position recorded at 25 °C. (b) A zoomed-in view to see variation in the amplitude of PM movement for frame 30–40 for all measurements PM position 1–10. (c) An average position of the PM was calculated and plotted with the standard deviation ( $\pm 0.85$  pixel) in the PM position, (d) thermal sag measurement, green and red curves, shows the movement of the proof mass at 25 and 45 °C respectively. The image frames were recorded at 20 frames per second (FPS).

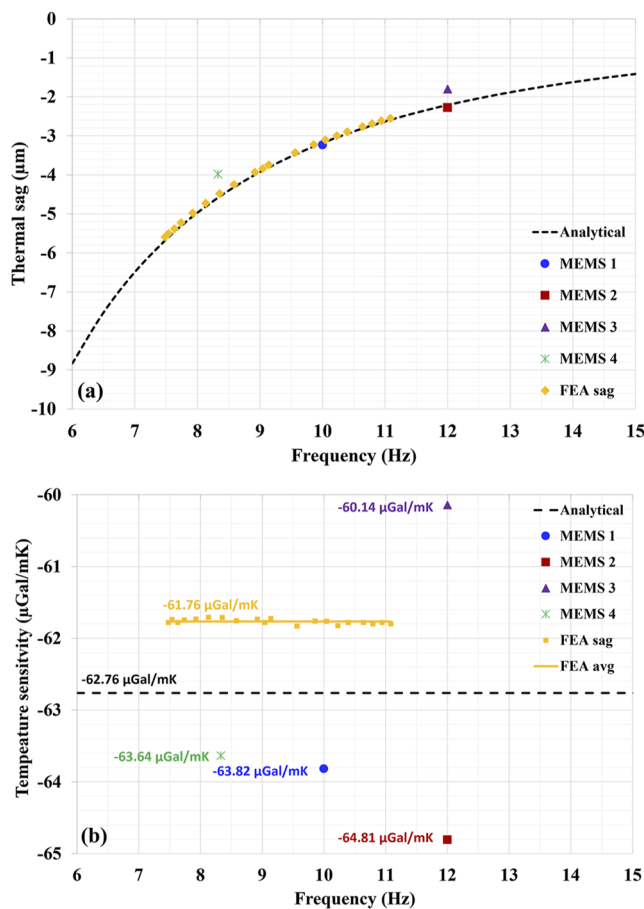


**FIG. 5.** (a) The thermal sag measurements and (b) temperature sensitivity of the MEMS gravimeter. The black dashed line shows an analytical estimate of the thermal sag of the MEMS gravimeter as a function of frequency. The yellow diamond points are thermal sags calculated using the FEA. The solid blue circle, purple triangular, and red square symbols are the thermal sag measured by changing the temperature from 25 to 45 °C of the MEMS gravimeter. The thermal sag measurements were conducted for a 20 °C change in the temperature.

inherent material properties used for the MEMS device's fabrication. If the silicon material properties can be tuned, then it is possible to make temperature insensitive MEMS gravimeters.

## V. CONCLUSION

This paper demonstrates the performance of MEMS gravimeters under the influence of temperature. It demonstrates the significance of the thermal sag of MEMS gravimeters on a device that can measure gravity changes of a few 10 s of μGal. It has also presented a bespoke optical measurement setup to quantify the thermal sag of MEMS devices. Such measurements preclude the requirement for integrating a complete packaged device using electronics and/or using more expensive instrumentation to be able to extract the thermal sensitivity of the device. It is a low-cost, reliable, and easy-to-use measurement technique that measures the temperature sensitivity of

MEMS gravimeters quickly without device packaging and complex signal conditioning circuit. The results obtained from optical measurements show very close agreement with those of analytical and FEA calculations. Such a measurement system is required before any implementation of a suitable compensation technique to mitigate the temperature induced effects of the devices can be verified.

## ACKNOWLEDGMENTS

This work was funded by the UK National Quantum Technology Hubs in Quantum Enhanced Imaging (Grant No. EP/M01326X/1), Sensing and Timing (Grant No. EP/T001046/1), NEWTON-g project funded by the EC's Horizon 2020 program, under the FETOPEN-2016/2017 call (Grant Agreement No. 801221) and Royal Academy of Engineering Grant Nos. CiET2021\_123 and RF/201819/18/83.

## AUTHOR DECLARATIONS

### Conflict of Interest

The authors have no conflicts to disclose.

### Author Contributions

**Vinod Belwanshi:** Conceptualization (equal); Formal analysis (equal); Funding acquisition (equal); Investigation (equal); Methodology (equal); Project administration (equal); Validation (equal); Writing – original draft (equal); Writing – review & editing (equal). **Abhinav Prasad:** Conceptualization (equal); Writing – review & editing (equal). **Karl Toland:** Formal analysis (supporting); Writing – review & editing (supporting). **Richard Middlemiss:** Writing – review & editing (supporting). **Douglas Paul:** Funding acquisition (equal); Writing – review & editing (equal). **Giles Hammond:** Conceptualization (equal); Funding acquisition (equal); Writing – review & editing (equal).

## DATA AVAILABILITY

The data that support the findings of this study are available from the corresponding authors upon reasonable request.

## REFERENCES

- R. P. Middlemiss, A. Samarelli, D. J. Paul, J. Hough, S. Rowan, and G. D. Hammond, *Nature* **531**(7596), 614 (2016).
- A. Prasad, S. G. Bramsiepc, R. P. Middlemiss, J. Hough, S. Rowan, G. D. Hammond, and D. J. Paul, "A portable MEMS gravimeter for the detection of the Earth tides," in *2018 IEEE Sensors* (IEEE, New Delhi, India, 2018).
- R. P. Middlemiss, P. Campsie, W. Cunningham, R. Douglas, V. McIvor, V. Belwanshi, J. Hough, S. Rowan, D. J. Paul, A. Prasad, and G. D. Hammond, in *Proceedings of 2022 IEEE International Symposium on Inertial Sensors and Systems* (IEEE, 2022).
- V. Belwanshi, A. Prasad, K. Toland, K. Anastasiou, S. Bramsiepc, R. Middlemiss, D. J. Paul, and G. D. Hammond, in *Proceedings of 2022 IEEE International Symposium on Inertial Sensors and Systems* (IEEE, 2022).
- R. Melamud, S. A. Chandorkar, B. Kim, H. K. Lee, J. C. Salvia, G. Bahl, M. A. Hopcroft, and T. W. Kenny, *J. Microelectromech. Syst.* **18**, 1409 (2009).
- M. A. Hopcroft, W. D. Nix, and T. W. Kenny, *J. Microelectromech. Syst.* **19**, 229 (2010).

- <sup>7</sup>C. Bourgeois, J. Hermann, N. Blanc, N. F. de Rooij, and F. Rudolf, "Determination of the elastic temperature coefficients of monocrystalline silicon," in *Proceedings of the International Solid-State Sensors and Actuators Conference - TRANSDUCERS '95* (IEEE, Stockholm, Sweden, 1995).
- <sup>8</sup>B. A. Boom, A. Bertolini, E. Hennes, R. A. Brookhuis, R. J. Wiegerink, J. F. J. van den Brand, M. G. Beker, A. Oner, and D. van Wees, in *Proceedings of the IEEE International Conference on Micro Electro Mechanical Systems (MEMS)* (IEEE, 2017), Vol. 33.
- <sup>9</sup>H. Zhang, X. Wei, Y. Gao, and E. Cretu, *J. Micromech. Microeng.* **30**, 085014 (2020).
- <sup>10</sup>G. Cella, V. Sannibale, R. Desalvo, S. Márka, and A. Takamori, *Nucl. Instrum. Methods Phys. Res., Sect. A* **540**, 502 (2005).
- <sup>11</sup>M. Blom, "Seismic attenuation for advanced Virgo vibration isolation for the external injection bench," Ph.D. thesis, Vrije Universiteit, Amsterdam, The Netherlands, 2015.
- <sup>12</sup>P. Kamp, "Towards an ultra sensitive seismic accelerometer," M.S. thesis, University of Twente, The Netherlands, 2015.
- <sup>13</sup>H. Liu, W. T. Pike, C. Charalambous, and A. E. Stott, *Phys. Rev. Appl.* **12**, 064057 (2019).
- <sup>14</sup>D. Carbone, L. Antoni-Micollier, G. Hammond, E. de Zeeuw-van Daltsen, E. Rivalta, C. Bonadonna, A. Messina, J. Lautier-Gaud, K. Toland, M. Koymans, K. Anastasiou, S. Bramsiepe, F. Cannavò, D. Contrafatto, C. Frischknecht, F. Greco, G. Marocco, R. Middlemiss, V. Ménoret, A. Noack, L. Passarelli, D. Paul, A. Prasad, G. Siligato, and P. Vermeulen, *Front. Earth Sci.* **8**, 573396 (2020).
- <sup>15</sup>K. Toland, "Aspects of fused silica fibres for use in gravitational waves research," Ph.D. thesis, University of Glasgow, Glasgow, UK, 2020.
- <sup>16</sup>J. Schindelin, I. Arganda-Carreras, E. Frise, V. Kaynig, M. Longair, T. Pietzsch, S. Preibisch, C. Rueden, S. Saalfeld, B. Schmid, J.-Y. Tinevez, D. J. White, V. Hartenstein, K. Eliceiri, P. Tomancak, and A. Cardona, *Nat. Methods* **9**(7), 676 (2012).